Talanta 208 (2020) 120437

Contents lists available at ScienceDirect

Talanta

journal homepage: www.elsevier.com/locate/talanta

Organic molecule-assisted synthesis of Fe_3O_4/graphene oxide nanocomposites for selective capture of low-abundance peptides and phosphopeptides

Jia-yuan Li[a], Xing-yu Long[a,b], Dong Sheng[a], Hong-zhen Lian[a,*]

[a] State Key Laboratory of Analytical Chemistry for Life Science, Collaborative Innovation Center of Chemistry for Life Sciences, School of Chemistry & Chemical Engineering and Center of Materials Analysis, Nanjing University, 163 Xianlin Avenue, Nanjing, 210023, China
[b] School of Chemistry and Materials Science, Guizhou Normal University, 180 Baoshan North Road, Guiyang, 550001, China

ARTICLE INFO

Keywords:
Fe_3O_4/GO probe
Organic molecule-assisted method
Low-abundance peptides
Phosphopeptides
Sequential enrichment
MALDI-TOF MS

ABSTRACT

The iron oxide nanoparticles (Fe_3O_4) were prepared by organic molecule-assisted method in aqueous solution. The facile synthetic process of Fe_3O_4 nanoparticles was conducted only by mixing $FeCl_2$ and 2-methylimidazole (2-MIM) without any additives. A possible growth mechanism of the Fe_3O_4 nanocrystals was proposed for this mild reaction. Then, the Fe_3O_4 nanoparticles were anchored onto graphene oxide (GO) sheets in water by ultrasound-assisted method, forming an affinity probe with strong biocompatibility. Due to the hydroxy and carboxylic groups of GO sheets, Fe_3O_4/GO probe exhibits excellent performance for enriching low-abundance hydrophilic peptides, while the Fe_3O_4 nanoparticles endure the probe with specific affinity to phosphopeptides. The analytical protocol was developed for sequential enrichment of low-abundance peptides and phosphopeptides by the affinity probe. It exhibited the sequence coverage of 26% for capture of 17 low-abundance peptides from bovine serum albumin (BSA), as well as the selectivity of 1:1:100 for phosphopeptides from α-/β-casein/BSA, and low detectable concentration of 2.5 fmol and probe reusability of 5 times for capture of phosphopeptides from α-/β-casein. Consequently, the prepared Fe_3O_4/GO material possesses excellent feature as multifunctional affinity probe for low-abundance peptides including phosphopeptides from complex biological matrices detected by matrix-assisted laser desorption ionization time-of-flight mass spectrometry.

1. Introduction

As well known, many endogenous peptides provide valuable information for revealing various diseases and illuminating pathological variations [1,2]. In particular, protein phosphorylation plays a crucial role in signal transduction, metabolism, cell cycle control, proliferation and differentiation [3]. As a powerful soft ionization technique, matrix-assisted laser desorption ionization time-of-flight mass spectrometry (MALDI-TOF MS) is especially suitable for analysis of peptides/proteins [4]. Nevertheless, it is still arduous and difficult for direct analysis of the low-abundance peptides/phosphopeptides in MALDI-TOF MS. Primarily, these peptides in real biological samples remain extremely low concentrations. Besides, abundant proteins/peptides as well as other impurities (salts and surfactants) generate serious interference and suppression in peptides analysis [5]. Moreover, the detection of phosphopeptides by MS analysis continuously suffers from the low ionization efficiency of phosphopeptides due to the negative phosphate groups [6]. Thus, it is indispensable to selectively enrich low-abundance peptides including phosphopeptides from biological samples with proper sampling procedures before MALDI-TOF MS analysis [7,8].

Until now, diversified sample pre-treatment techniques based on functional magnetic materials have been explored for analysis of low-abundance peptides/phosphopeptides, which could achieve better separation than conventional approaches [9]. Notably, various core-shell structured magnetic materials have been prepared and applied for the enrichment of low-abundance peptides [10–19]. As mentioned in above reports, the acting sites of functional magnetic materials for pre-concentration of low-abundance peptides are principally based on carbon material shells. Meanwhile, related researches affirmed that the main driving forces for the affinity between peptides/proteins and carbon nanomaterials are ascribed to hydrophobic and π-π stacking interactions. Otherwise, for capturing and isolating phosphopeptides, various attractive functional magnetic materials have been developed [20–32]. Among these affinity materials, the high sensitive and selective

* Corresponding author.
E-mail address: hzlian@nju.edu.cn (H.-z. Lian).

https://doi.org/10.1016/j.talanta.2019.120437
Received 11 May 2019; Received in revised form 28 September 2019; Accepted 3 October 2019
Available online 18 October 2019
0039-9140/

combination with phosphate groups by metal oxide nanoparticles relies on the robust Lewis acid-base interaction. Recently, some bare or doped magnetic ferrites, including γ-Fe_2O_3, Fe_3O_4, $NiFe_2O_4$, $ZnFe_2O_4$, $MnFe_2O_4$ etc. [33–35], which combine merits of magnetic property and solid Lewis acid function, have been exploited for capturing phosphopeptides. However, from the thermodynamic point of view, these nanoscale particles are potentially unstable because of their high surface energy [36]. It trends to aggregate and form large particles due to anisotropic dipolar interactions in aqueous solution, which decreases their dispersivity and specific surface, and diminishes their merits for phosphopeptides enrichment. Therefore, it is significant to immobilize these nanoparticles onto certain supports to prevent their aggregations.

Furthermore, some newly developed affinity materials were used to enrich low-abundane peptides and phosphopeptides simultaneously. For instance, Bai and Liu's group developed a multifunctional composite (r-GO-SnO_2 NRs) for sequential capturing low-abundance peptides and phosphopeptides prior to MS detection [37]. Zhang's group fabricated CeO_2//SiO_2–C_8 Janus fiber and magnetic $LaPO_4$-*r*-GO affinity probe (LaGM) to isolate low-abundance peptides and phosphopeptides for MS detection [38,39]. However, the preparation procedures of above delicate affinity probes are relatively time-consuming. It is somewhat tedious for the enrichment process with r-GO-SnO_2 and CeO_2//SiO_2–C_8 Janus fiber due to centrifugation compared with magnetic separation. In addition, both r-GO-SnO_2 and LaGM composites are graphene-based materials, which often exhibit weak dispersibility owing to the hydrophobic graphene part. That is perhaps unfavorable for the analysis of low-abundance hydrophilic peptides including phosphopeptides. Moreover, the reciprocal superposition of the affinity site of $LaPO_4$ may act against hydrophobic graphene during the capture and isolation of hydrophilic low-abundance peptides and phosphopeptides. However, the hydroxyl and epoxy groups of hydrophilic graphene oxide (GO) offer numerous active sites for the modification of functional materials such as Fe_3O_4 [40,41]. Apart from huge specific surface, high-load capacity and unique large delocalized π-π electron system, GO is equipped with excellent biocompatibility and stability, which can strongly interact with proteins/peptides via H-bonding and electrostatic interaction or π-π interaction, therefore providing a highly efficient platform for low-abundance peptides enrichment.

Fe_3O_4 nanoparticles have received considerable attention for the development of biomedical applications compared with other higher magnetic materials [42]. Furthermore, some factors are significant for their biomedical application. For instance, narrow size distributions and micro-size below 100 nm of Fe_3O_4 nanoparticles are propitious to minimize sedimentation, reduce the dipolar interaction between nanoparticles, and facilitate tissular diffusion [43]. Many synthesis routes, including solvothermal method, thermal decomposition method, sol-gel method and co-precipitation method [44–49], have been explored for fabricating Fe_3O_4 particles. Solvothermal method was firstly reported by Li's group [44], which is easily controlled and could produce uniform nanoparticles. However, this tedious method is arduous to acquire small nanoparticles. Thermal decomposition method offers great advantages of obtaining the monodisperse particles with magnetic susceptibility owing to higher crystallinity degree and purer phases, which has a facile scaling-up possibility. However, the resultant nanoparticles synthesized via this method are hydrophobic and need further surface modification for further application in bioanalysis. Sol-gel method in aqueous matrix has an additional advantage for biomedical application without further surface modification. However, it is also a little bit time-consuming. The co-precipitation method, which is a reaction in alkali media entailed stoichiometric mixtures of ferrous and ferric hydroxides [48], can produce abundant Fe_3O_4 nanoparticles. However, it is difficult to control the temperature and pH of reaction. Therefore, a facile, timesaving and reliable approach to prepare this material at an affordable cost is desirable for large-scale application.

In this present work, a facile strategy to fabricate Fe_3O_4 affinity materials was developed in aqueous solution by 2-methyl imidazole (2-MIM) -assisted method. The structure of 2-MIM is shown in Fig. S1. Meanwhile, a possible growth mechanism of the Fe_3O_4 nanocrystals was proposed preliminarily. In addition, as-prepared Fe_3O_4 nanoparticles were uniformly decorated onto hydrophilic GO nanosheets through ultrasonic-assisted method. Notably, the possibility of the Fe_3O_4/GO nanocomposites were explored to be utilized as bifunctional affinity probe not only for effectively enriching low-abundance peptides based on the integrated interaction from the unique property of GO, but also for selectively capturing phosphopeptides form complex biosamples in virtue of the affinity of Fe_3O_4 nanoparticles.

2. Experimental

2.1. Materials and reagent

2-Methylimidazole (2-MIM) and ammonium bicarbonate (NH_4HCO_3) were obtained from Aladdin Chemical (Shanghai, China). Ferric chloride ($FeCl_3·H_2O$), ferrous chloride ($FeCl_2·4H_2O$) and ammonium solution ($NH_3·H_2O$) (28%, w/w) were purchased from Nanjing Chemical Reagent (Nanjing, China). Bovine serum albumin (BSA, MW = 67 kDa), angiotensin II (MW = 1046.2 Da), bovine α-/β-casein (MW = 25 kDa), phosphoric acid (85%, w/w), 2,5-dihydroxybenzoic acid (DHB) (puriss p.a.), trifluoroacetic acid (TFA) and acetonitrile (ACN) of HPLC grade were offered by Sigma-Aldrich (St. Louris, MO, USA). Sequencing grade modified trypsin was obtained from Promega (Madison, WI, USA). Commercial ZipTipC18 pipette tips were supplied by Millipore (Billerica, MA, USA). All the chemical agents were analytical grade unless otherwise noted and used without further purification. Ultrapure water was from a Milli-Q system (Millerica, USA). Human urine and serum samples were ungrudgingly provided by healthy volunteers. The study was approved by the Medical Ethical Committee of the First Affiliated Hospital of Nanjing Medical University. Nonfat milk was bought from an Education Supermarket in Xianlin campus of Nanjing University (Nanjing, China) within 24 h before the experiment and used during the shelf-life. All samples were stored in a refrigerator at −80 °C prior to treatment.

2.2. Preparation of superparamagnetic Fe_3O_4 nanoparticles and Fe_3O_4/GO nanocomposites

A schematic representation of the synthesis procedure of Fe_3O_4 and Fe_3O_4/GO displays in Scheme 1A. $FeCl_2·4H_2O$ (127.5 mg, 0.6 mmol) was solubilized in the 5 mL water, and 2-MIM (1.642 g, 2 mmol) was solubilized in another 15 mL water. For synthesis of the Fe_3O_4 nanoparticles, these two solutions were mixed vigorously by vortex for 60 s, then, the obtained solution was incubated for another 30 min at room temperature. Finally, the resulting black Fe_3O_4 precipitates were collected with the external magnetic field, and then rinsed with water and ethanol in turn, and dried at 60 °C for further use.

According to previous reports with minor modification [40], Fe_3O_4/GO nanocomposites were prepared by assembling Fe_3O_4 nanoparticles onto GO nanosheets. Briefly, 5 mg of GO nanosheets were dispersed in water via ultrasonication for 60 min to form GO suspension at a concentration of approximately 1 mg mL^{-1}. Then, 10 mL of Fe_3O_4 suspension (10 mg mL^{-1}) was slowly injected into GO dispersion system with the assistance of sonication and further mechanical stirred for 60 min to obtain magnetic Fe_3O_4/GO nanocomposites.

2.3. Characterization of materials

The characterization of as-prepared Fe_3O_4 nanoparticles and Fe_3O_4/GO nanocomposites were performed by transmission electron microscopy (TEM), scan electron microscopy (SEM), X-ray powder (XRD), Fourier-transform infrared spectroscopy (FT-IR), Raman microscope configuration, quantum design SQUID VSM magnetometer as well as nitrogen adsorption-desorption measurements. The detailed

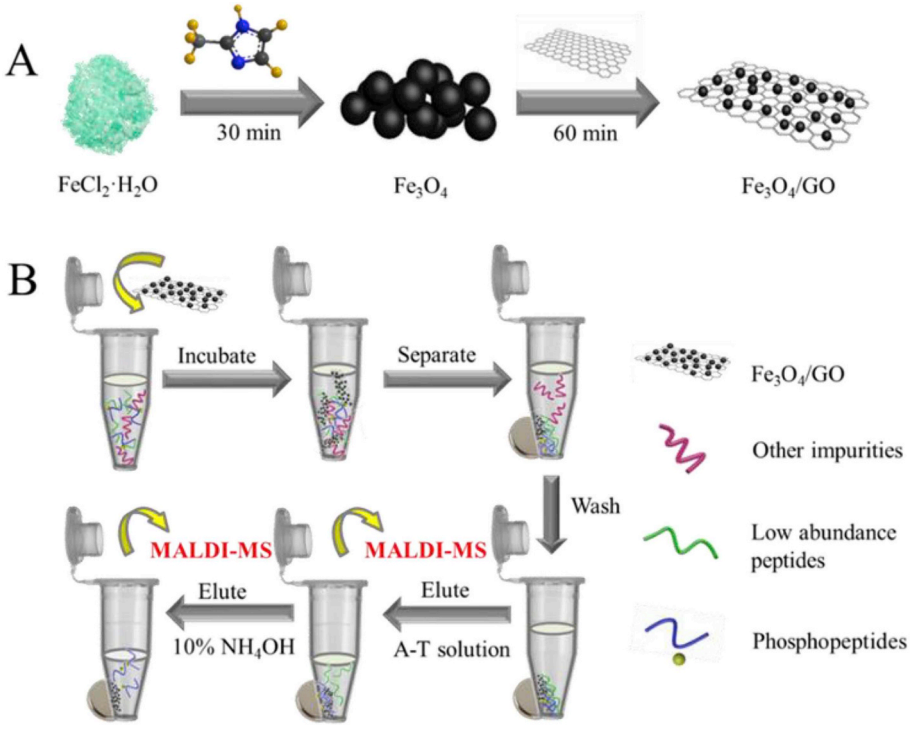

Scheme 1. Schematic illustration of the synthesis strategy of Fe_3O_4/GO nanocomposites (A), and the procedure for capture and labeling of low-abundance peptides and phosphopeptides (B).

information of apparatus and characterization are listed in the electronic supplementary material.

2.4. Protein digestion

The digests of standard α-/β-casein, BSA and nonfat milk, human serum were prepared according to our previous work [29]. Briefly, standard α-/β-casein or BSA (1 mg) was dissolved in 1.0 mL of NH_4HCO_3 aqueous solution (50 mM, pH 8.3), respectively. Then, trypsin was added into the solution with a molar ratio of 1:50 (trypsin/substrate) at 37 °C for 18 h. Afterwards, the obtained tryptic digests were diluted to the target concentration with aqueous solution of 50% ACN and 2% TFA (v/v, denoted as A-T solution) or water, respectively. 30 μL nonfat milk was 30-fold diluted by 50 mM NH_4HCO_3 aqueous solution, followed by centrifugation at speed of 14000 rpm for 10 min. Then, the albuminous supernatant was degenerated at 100 °C for 15 min. Subsequently, 80 μL of trypsin (20 μg mL^{-1}) was added for proteolysis at 37 °C for 16 h. Before analysis, the frozen digests at −80 °C were thawed and then diluted to suitable concentration with A-T solution or water.

2.5. Enrichment of low-abundance peptides

BAS digest was diluted to 10 nM with water, angiotensin II was prepared in water (5 nM, pI = 6.74), and human urine was diluted 10-fold with water. Then, 500 μL of sample solution was mixed with 5 μL of 20 mg mL^{-1} Fe_3O_4/GO nanocomposites suspending solution and vortexed for 10 min. Subsequently, the composites with trapped peptides were isolated via magnetic separation, and washed with 500 μL of water twice to remove unbound impurities. Afterwards, the target peptides were eluted with 5.0 μL of A-T solution (60% ACN, 1% TFA), and the supernatant was collected for MALDI-TOF MS analysis.

2.6. Enrichment of phosphopeptides

Digests of α-/β-casein were diluted to 10 pmol with A-T solution, and digest of nonfat milk was diluted 30-fold with A-T solution. Then, 100 μL of sample solution was mixed with 5 μL of 20 mg mL^{-1} Fe_3O_4/GO nanocomposites. Then, Fe_3O_4/GO affinity probe loaded with phosphopeptides was separated with a magnet after vortex for 30 min. After wash by A-T solution three times to remove impurities, the trapped phosphopeptides were eluted with 5.0 μL of 10 wt% $NH_3 \cdot H_2O$ by ultrasonication for 10 min. Finally, the supernatant was taken out by magnetic separation for MS analysis.

2.7. Stepwise enrichment of low-abundance peptides and phosphopeptides in human serum

The workflow to sequential enrichment of low-abundance peptides and phosphopeptides is illustrated in Scheme 1B. 10 μL of human serum was diluted 20-fold by water to form a uniform solution. 5 μL of 20 mg mL^{-1} Fe_3O_4/GO nanocomposites were mixed with the 500 μL of sample solution and then vortexed for 10 min. Thereafter, nanocomposites loaded with peptides were rinsed three times with 100 μL of water for eliminating unspecific adsorption. Afterwards, the trapped low-abundance peptides were eluted with 5.0 μL of A-T solution, and the supernatant was collected by magnetic separation for MALDI-TOF MS detection. Subsequently, the retained phosphopeptides were eluted with 5.0 μL of 10 wt% $NH_3 \cdot H_2O$ for MALDI-TOF MS analysis.

2.8. MALDI-TOF MS analysis

All the MALDI-TOF MS experiments were carried out in a reflector positive ion mode on a 4800 Plus MALDI TOF/TOF TM analyzer (Applied Biosystems, USA) with the Nd-YAG laser at 355 nm and an acceleration voltage of 20 kV [35]. The MALDI-TOF mass spectrometer used a ground-steel sample target plate with 384 spots. 20 mg mL^{-1} DHB (in 50% ACN/water containing 1% H_3PO_4 solution, v/v) was used as the matrix for the analysis of peptides by MALDI-TOF MS. Sample aliquots (0.5 μL) were placed on the MALDI plate and dried at room temperature. After adding DHB matrix (0.5 μL), the sample spots were dried under vacuum prior to TOF-MS analysis.

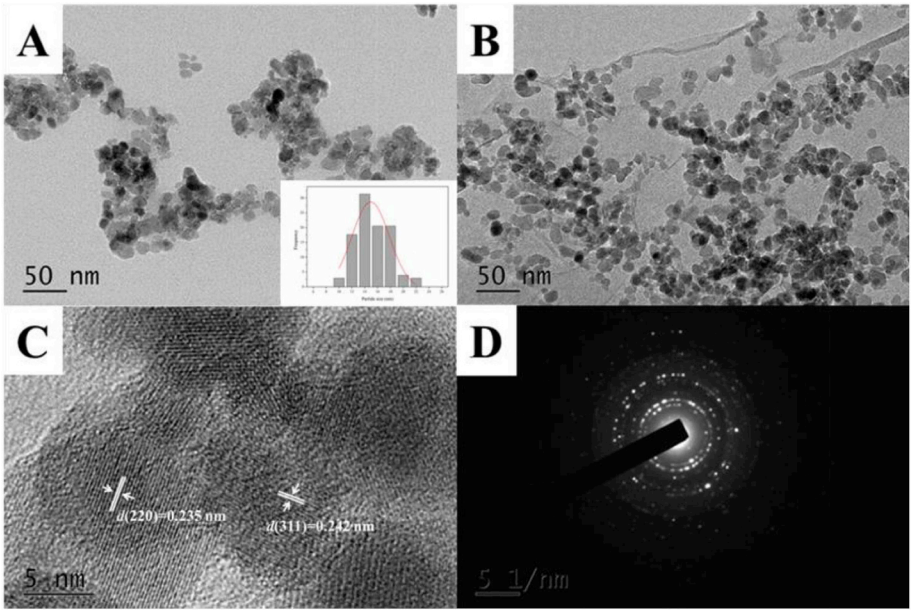

Fig. 1. TEM images of Fe_3O_4 (A) and Fe_3O_4/GO (B), HRTEM images (C) and SAED pattern (D) of Fe_3O_4 nanoparticles. The inset image shows size distribution of Fe_3O_4 nanoparticles.

The obtained mass spectrometry raw data were processed via ProteinPilot 4.0 software (AB SCIEX) with the Paragon search mode. Trypsin was set as the specific proteolytic enzyme and a maximum of two missed cleavages were allowed for the analysis. Phosphorylation modification emphasis was selected as a search parameter. The precursor tolerance was set to 1.5 Da. Proteins were identified using MASCOT search engine (database: SwissProt; digested used: trypsin; maximum of missed cleavages: 1; mass tolerance: ± 50 ppm).

3. Results and discussion

3.1. Synthesis and characterization of Fe_3O_4/GO affinity probe

Herein, we conducted a simple and high yield organic molecule-assisted method to synthesize Fe_3O_4 nanoparticles. That is, $FeCl_2$, used as the source of ferrous ion, was mixed with 2-MIM in water to obtain black Fe_3O_4. The possible formation mechanism of Fe_3O_4 is elucidated in supplementary material. Afterwards, Fe_3O_4 nanoparticles were assembled onto GO surface by mixing GO and Fe_3O_4 solutions with ultrasound-assistant method to obtain Fe_3O_4/GO affinity probe materials.

Fig. 1 shows the TEM images of Fe_3O_4 nanoparticles and Fe_3O_4/GO nanocomposites. The mean grain size of approximately spherical-shaped Fe_3O_4 nanocrystals was nearly 15 nm (see Fig. 1A, inset). The satisfactory shape and size of the nanostructure profited from the assistance of organic 2-MIM in preparation process. Then, the surface-bound nanocomposites Fe_3O_4/GO were formed by ultra-distributed Fe_3O_4 nanoparticles on GO sheets (Fig. 1B), which is attributed to many oxygenated functional groups, such as epoxy, hydroxyl and carboxyl on the surface of GO sheets [40]. Fe_3O_4/GO still retained well the 2D nanostructure of GO sheets. Moreover, the fringe spacing of 0.235 nm and 0.242 nm (Fig. 1C) observed from HRTEM image matched the *d* (220) and *d*(440) planes of Fe_3O_4 nanoparticles. Moreover, the polycrystalline of Fe_3O_4 crystal was confirmed in the selected area electron diffraction (SAED) pattern (Fig. 1D).

In addition, the phase of as-prepared Fe_3O_4 nanoparticles was attributed to Fe_3O_4 on account of their Raman shifts at around 305, 528 and 663 cm^{-1} (Fig. S2) [32,50]. The phase composition and the crystallite size of Fe_3O_4 nanoparticles and Fe_3O_4/GO nanocomposites were determined by XRD spectra in Fig. S3. The planes (111), (220), (311), (400), (422), (511) and (440) of Fe_3O_4 and Fe_3O_4/GO overlapped the standard XRD data card of Fe_3O_4 crystal [29] which indicated that the high crystalline state of Fe_3O_4 retained in the synthesized Fe_3O_4/GO probe. The functional groups of the Fe_3O_4 nanoparticles and Fe_3O_4/GO composites were studied using FT-IR spectra (Fig. S4). The broad peak at 3409 cm^{-1} was attributed to surface hydroxyl group. The peaks at 1730 cm^{-1} and 1560 cm^{-1} corresponded to the C═O stretching vibration and O–H bending of carbonyl COO^- group. The peak at 1190 cm^{-1} represented epoxy C–O symmetric vibration of GO sheets. The peak at 567 cm^{-1}, which was ascribed to Fe–O stretching vibration, indicated that Fe_3O_4 nanoparticles were successfully anchored onto the GO sheets. However, the strength of Fe–O stretching peak decreased for Fe_3O_4/GO affinity probe owing to the effect of non-magnetization component GO.

The magnetic hysteresis loops of Fe_3O_4 nanoparticles and Fe_3O_4/GO composites are displayed in Fig. S5, indicating that both of the materials manifested typical superparamagnetic property. The saturation magnetization of Fe_3O_4/GO nanocomposites (25.0 emu g^{-1}) was lower than that of Fe_3O_4 nanoparticles (77.6 emu g^{-1}) mainly due to the presence of non-magnetic GO sheets. The superparamagnetic performance suggested that Fe_3O_4/GO affinity probe can be rapidly isolated by a magnet. Meanwhile, Fe_3O_4/GO can be dispersed again into solution after removing the magnetic field. In order to estimate the porous structure and surface area of Fe_3O_4/GO composites, N_2 adsorption-desorption isotherms were drawn as shown in Fig. S6. The BET surface area of the Fe_3O_4/GO was calculated 96.05 $m^2 g^{-1}$. Obviously, Fe_3O_4/GO nanocomposites possessed much higher specific surface area than Fe_3O_4 nanoparticles (51.44 $m^2 g^{-1}$) owing to the GO sheets involved. The contact angle values of the prepared Fe_3O_4 nanoparticles and Fe_3O_4/GO nanocomposites were measured to be 53.2° and 33.8°, respectively (Fig. S7). Such results indicated that Fe_3O_4 nanoparticles were relatively hydrophilic. Moreover, the hydrophilicity was substantially improved after Fe_3O_4 nanoparticles were anchored on GO sheets.

3.2. Feasibility evaluation of Fe_3O_4/GO probe in enrichment of low-abundance peptides

BSA tryptic digest (10 nM) was employed as a model sample (Fig. 2). Only four peptides were observed by direct analysis (Fig. 2A). After capture and isolation with the Fe_3O_4/GO probe, 17 peptides were

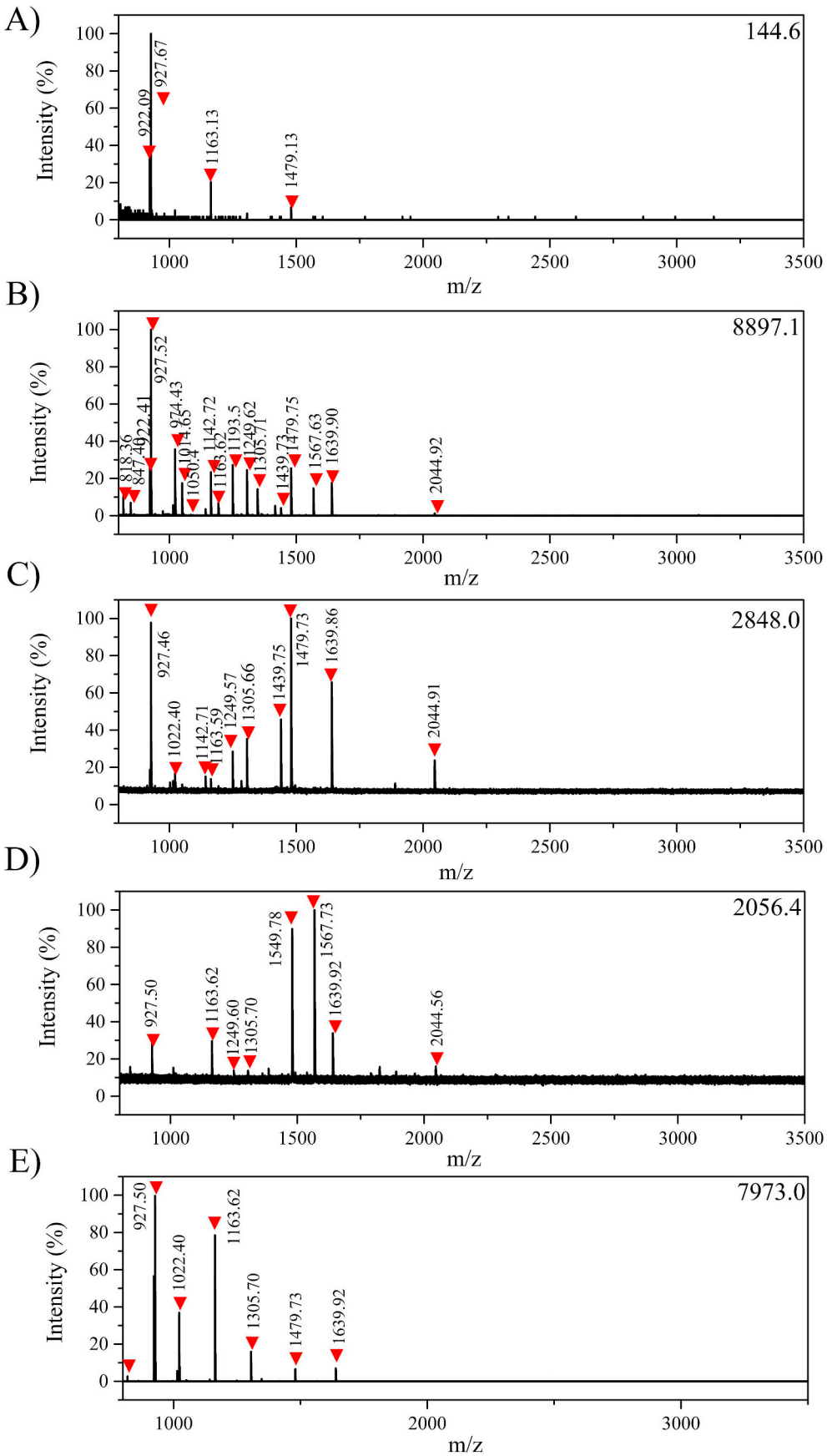

Fig. 2. Mass spectra of (10 nM) BSA digest treated with different materials: A. without treatment; B. Fe_3O_4/GO affinity probe; C. Fe_3O_4 nanoparticles; D. commercial ZiptipC18. "▼" represents low-abundance peptides. The number in the upper right corner represents the strongest peak intensity.

Table 1
The search results of 10 nM BSA digests before and after enrichment with Fe_3O_4/GO nanocomposites.

Position	Calc. m/z	Peptide sequences	pI	GRAVY	Before	After
562–568	818.3	ATEEQLK	4.53	−1.36		+
242–248	847.4	LSQKFPK	10.00	−1.01		+
249–256	922.4	AEFVEVTK	4.53	0.18	+	+
161–167	927.5	YLYEIAR	6.00	−0.07	+	+
37–44	974.4	DLGEEHFK	4.65	−1.10		+
549–557	1014.6	QTALVELLK	6.00	0.64		+
588–597	1050.4	EACFAVEGPK	4.53	0.02		+
548–557	1142.7	KQTALVELLK	8.59	0.19		+
66–75	1163.6	LVNELTEFAK	4.53	0.13	+	+
25–34	1193.5	DTHKSEIAHR	6.92	−1.70		+
35–44	1249.6	FKDLGEEHFK	5.45	−1.25		+
402–412	1305.7	HLVDEPQNLIK	5.32	−0.58		+
360–371	1439.7	RHPEYAVSVLLR	8.75	−0.13		+
421–433	1479.7	LGEYGFQNALIVR	6.00	0.29	+	+
437–451	1567.6	DAFLGSFLYEYSR	4.37	−0.09		+
413–427	1639.9	KVPQVSTPTLVEVSR	8.75	−0.067		+
168–183	2044.9	RHPYFYAPELLYYANK	8.39	−0.812		+
	Match				4	17
	Coverage				N.D.	26%

measured by MS detection with the sequence coverage of 26% (Fig. 2B). Table 1 lists the corresponding peptide sequences of these ions. It is worthwhile to note that the grand average of hydropathy (GRAVY) value of 12 peptides among all 17 peptides is negative, which implies that these peptides are hydrophilic. This is mostly due to synergic action including hydrophilic interaction, hydrogen-bond interaction and electrostatic interaction between low-abundance peptides and graphene oxides. In brief, the above results showed the advantage of the as-prepared Fe_3O_4/GO probe in enrichment of low-abundance peptides. As a comparison, after treatment with Fe_3O_4 nanoparticles (Fig. 2C) and ZipTipC18 (Fig. 2D), only 10 and 8 peptides were detected from the BSA tryptic digest respectively, indicating that the novel Fe_3O_4/GO affinity probe possesses a universality towards low-abundance peptides.

A standard peptide, angiotensin II was chosen as a model sample (Fig. S7). Before enrichment, angiotensin II (5 nM) was barely detectable with low signal-to-noise (S/N) ratio less than 20 (Fig. S8A). After capture by Fe_3O_4/GO affinity probe, the peak intensity raised sharply with the S/N ratio of 623.98 (Fig. S8B), and the enrichment factor was more than 30, indicating that Fe_3O_4/GO probe has a high efficiency of enrichment in peptide analysis. Contrastively, after treatment with commercial ZipTipC18 pipette tip (Fig. S8C), the S/N ratio merely increased to 39.93 with enrichment factor of around 2. Thus, the results indicated that the novel Fe_3O_4/GO affinity probe possesses high efficiency for low-abundance peptides.

Furthermore, Fe_3O_4/GO affinity probe was in an attempt to enrich and isolate peptides from human urine. Only two peaks with the poor MS signals were detectable due to the low concentration in diluted urine sample by direct detection (Fig. S9A). Then, several peaks of urine peptides with proper intensity and S/N ratio of MS signal were observed through a rapid enrichment process (Fig. S9B). In a few work, the procedures of enriching low-abundance peptides by prepared nanocomposite were unaffected by the negative effect and other contaminants existing in complex urea sample. These characters exposited the applicability of Fe_3O_4/GO probe in capture of low-abundance peptides from real biological samples.

3.3. Feasibility evaluation of Fe_3O_4/GO affinity probe in capture of phosphopeptides

To obtain the best performance of phosphopeptides enrichment for MALDI-TOF MS detection, tryptic digests of α-/β-casein (10 pmol, molar ratio 1:1) were exploited as models, and A-T solutions with different TFA and ACN concentrations were optimized as loading buffer. In general, acidity of the loading buffer is a key factor for selectively trapping peptides. As is well known to all, protonation of acidic residues will happen at low pH, and decrease the nonspecific bonding with acidic peptides. Nevertheless, a high TFA concentration will weaken effectiveness in capture of phosphopeptides due to the destruction of the nature of Fe_3O_4 decorated on GO sheet.

The influence of TFA on the enrichment of phosphopeptides was cheked at different concentrations (0.1%, 0.5%, 1.0%, 2.0% and 6.0%, respectively). As shown in Fig. S10, with the increment of TFA concentration in loading buffer, the signals of high abundant non-phosphopeptides in MS strongly declined, indicating TFA would facilitate the Fe_3O_4/GO affinity to capture and isolate phosphopeptides. However, when the concentration of TFA is up to 6.0%, both number and intensity of phosphopeptides in MS decreased. After all, 2.0% TFA was the optimum acidity of loading buffer. Besides, it is essential to select appropriate concentrations of ACN in A-T solution due to the reduction of hydrophobic interaction between affinity probe and non-phosphopeptides. Thus, we optimized ACN proportions for enrichment of phosphopeptides (Fig. S11). Compared Fig. S11B with S11A, the intensity of MS peaks at 50% ACN concentration was higher than that at 30% ACN, indicating that the peak intensity of phosphopeptides will raise with increasing ACN concentration. Nevertheless, when ACN at high proportions of 70% and 90%, the peaks of non-phosphopeptides, at m/z 1383.7 and m/z 1760.8 dominated the MS spectra (Figs. S11C and D). Thus, 50% ACN concentration was optimum proportion for the loading buffer. In short, the optimum A-T solution was chosen with 2.0% TFA in 50% ACN loading buffer for efficiently capturing phosphopeptides.

To assess the enrichment efficiency of Fe_3O_4/GO probe for isolation and capture of phosphopeptides under the optimal A-T solution, α-/β-casein (10 pmol each) tryptic digests were employed as model samples. As shown in Fig. 3A, only 2 phosphopeptides with low MS intensity were detected and non-phosphopeptides were sovereign before enrichment (Fig. 3A). After extraction with Fe_3O_4/GO affinity probe (Fig. 3B), 20 phosphopeptides with strong MS intensity were expected exclusive of the interference of non-phosphopeptides. This is because of selective affinity on ground of Lewis acid-base interaction between phosphate groups of phosphopeptides and Fe_3O_4 in Fe_3O_4/GO nanocomposites. We further identified them through the characteristic fragment ions of mass loss of 80 Da (marked with "#"). Table S1 lists corresponding peptide sequences of these ions. In addition, Fe_3O_4 nanoparticles was also used for enrichment experiment. The mass spectrum in Fig. 3C indicated that poor effect on trapping phosphopeptides was presumably due to the aggregation of Fe_3O_4 nanoparticles. Commercial TiO_2 were used for capture of phosphopeptides (under the optimum extraction condition from Figs. S12 and 13), and the efficiency of enriching phosphopeptides by TiO_2 was inferior to Fe_3O_4/GO affinity probe.

To further test the sensitivity, selectivity and recyclability of Fe_3O_4/GO probe for capture of phosphopeptides, several experiments were carried out as follows. Firstly, the different concentrations of α-/β-casein tryptic digests were mixed with Fe_3O_4/GO affinity probe to capture phosphopeptides (Fig. S14). One phosphopeptide could still be clearly observed even under 2.5 fmol of tryptic digests of α-/β-casein. Then, different amounts of BSA digest were added to tryptic digests of α/β-casein solution. As shown in Figs. S15A1, B1 and C1, with the increase of interfering substance BSA digest added, the signals of non-phosphopeptides dramatically raised and phosphopeptides were suppressed before enrichment. After capturing phosphopeptides by Fe_3O_4/GO probe at the mixture sample of protein digests, several phosphopeptides were detected preventing the influence of non-phosphopeptides (Figs. S15A2 and B2). When BAS digest was at the concentrations 100 folds that of α-/β-casein digests, seven phosphopeptides peaks were still observed, although the non-phosphopeptides peaks dominated the mass spectrum owing to the GO sheets part of the affinity probe (Fig. S15C3). Moreover, Fe_3O_4/GO affinity probe was recycled

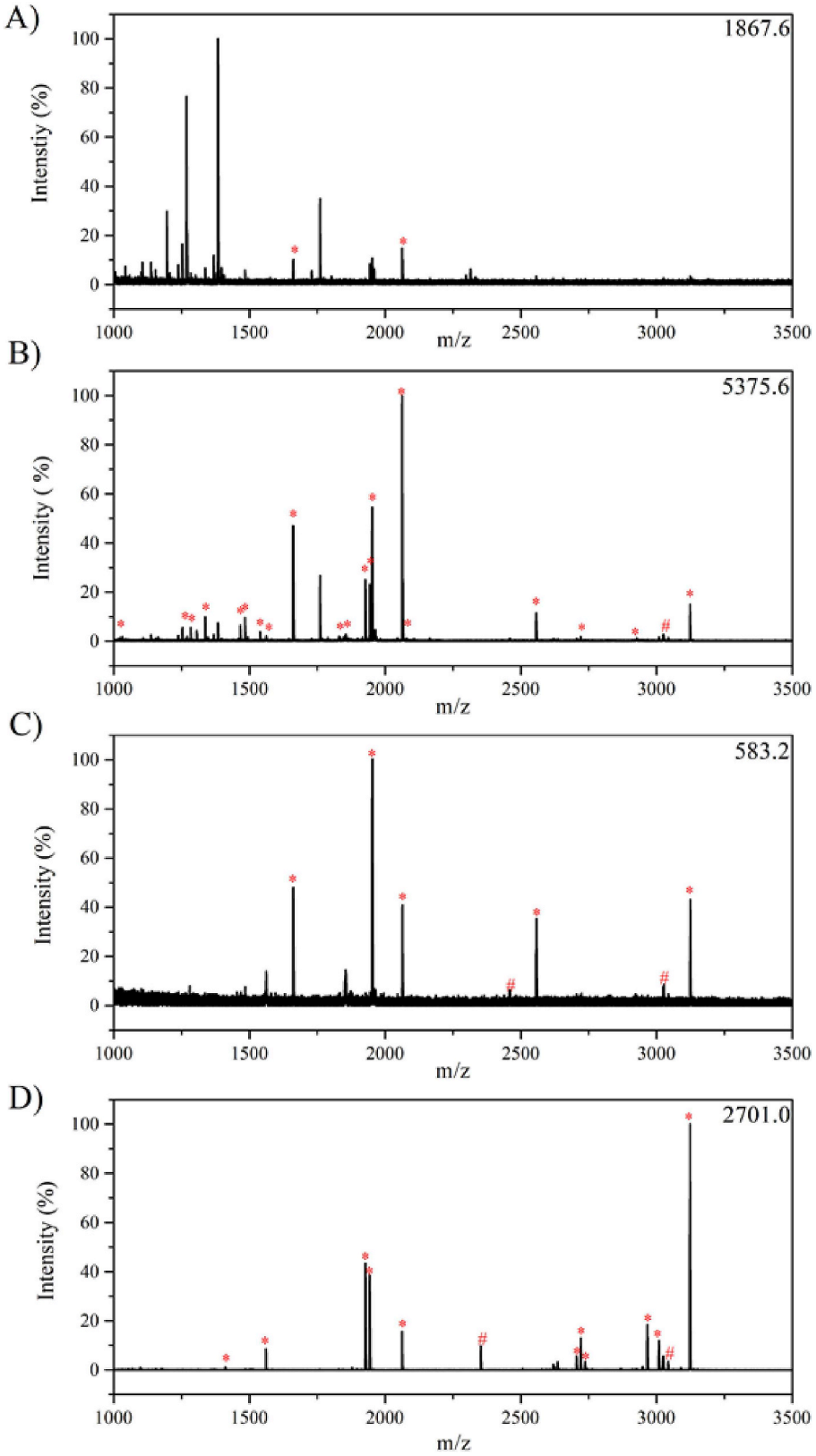

Fig. 3. Mass spectra of phosphopeptides from the trypsin digest of α-/β-casein (10 pmol, v/v = 1 : 1) treated with different materials: A. Before treatment; B. Fe_3O_4/GO; C. Fe_3O_4; D. TiO_2. "*" represents phosphpeptides or the corresponding doubly charged ions peaks; "#" represents the dephosphorylate fragments of phosphopeptides. The number in the upper right corner represents the strongest peak intensity.

for enrichment of phosphopeptides by washing with the A-T solution three times. As shown in Fig. S16, even after being regenerated for five times, the Fe_3O_4/GO affinity probe can still capture phosphopeptides effectively, and there was no obvious attenuation of peak intensity in MS spectra. On all accounts, the results manifested the high sensitivity, robust specificity as well as excellent reusability of the Fe_3O_4/GO

nanocomposites towards phosphopeptides.

To further estimate the performance of Fe_3O_4/GO affinity probe in practical application, nonfat milk was explored as a real sample for isolation of phosphopeptides. As shown in Fig. S17A, only four phosphopeptides with low peaks intensity were observable in the direct analysis. In contrast, after treated with Fe_3O_4/GO affinity probe, 15 phosphopeptides with high MS intensity can be easily observed free from interference of non-phosphopeptides (Fig. S17B). Table S2 lists the identified phosphopeptides enriched by Fe_3O_4/GO probe in the amino acid sequence pattern. These results illustrated the excellent applicability of Fe_3O_4/GO for phosphopeptides enrichment.

3.4. Simultaneous enrichment of the two kinds of target peptides in human serum

The analysis of endogenous peptides in human serum is significant for potential application of biological and pathological elucidation. However, it is still a challenge to detect endogenous peptides in serum by direct MS detection due to the highly dynamic nature, complexity as well as low peptide levels. Therefore, we applied the Fe_3O_4/GO affinity probe to capture low-abundance peptides and phosphopeptides stage by stage from serum sample before individual MS detection. Because of serious interference from the salts and other impurities as well as low peptide levels in serum, no peptides were identified before treatment of Fe_3O_4/GO probe (Fig. 4A). In contrast, after capture by Fe_3O_4/GO affinity probe, a large amount of endogenous peptides with strong MS peak intensity and S/N ratio appeared in MS spectrum (Fig. 4B) in the first elution step, which manifested good effect on trapping low-abundance peptides by Fe_3O_4/GO probe from real serum sample. More importantly, after second elution by 10 wt% ammonia, four phosphopeptides identified from serum were detectable, eliminating other influence of impurity and salts (Fig. 4C, Table S3). Meanwhile, ZipTipC18 pipette tips and TiO_2 nanoparticles were chosen for enrichment of the target peptides (low-abundance peptides and phosphopeptides, respectively) from human serum through the same extraction process (Fig. 4D and E). Obviously, these mono-functional commercial materials hardly execute multi-target enrichment. Moreover, the capability and efficiency of Fe_3O_4/GO affinity probe are superior to these two affinity probes for trapping the correspongding peptides. Overall, the Fe_3O_4/GO nanocomposites can efficiently extract these two kinds of target endogenous peptides step-by-step from real biological samples in individual MS detection.

3.5. Comparison with other bifunctional affinity materials

Detailed comparisons of the Fe_3O_4/GO affinity probe fabricated on the Fe_3O_4 nanoparticles that are synthesized by $FeCl_2$ and 2-MIM in aqueous solution with previously reported bifunctional affinity probes are shown in Table 2 in terms of amount of materials, separation mode, number of enriched peptides in BSA, limit of detection and enrichment selectivity for phosphopeptides, and application (tryptic digests). It is concluded that our Fe_3O_4/GO nanocomposites have comparable enrichment effects with these existing materials. In contrast to non-magnetic nanomaterials, magnetic separation endowed the enrichment process with a more convenient and rapid operation. This is likely because as-prepared Fe_3O_4 nanocrystals by facile organic molecule-assisted method are more uniform and anti-aggregative.

4. Conclusions

Fe_3O_4 nanocrystals were synthesized successfully by organic molecule-assisted method, mixing $FeCl_2$ and 2-methylimidazole (2-MIM) without any additives in aqueous solution. Meanwhile, a possible growth mechanism of the Fe_3O_4 nanostructure was proposed. The

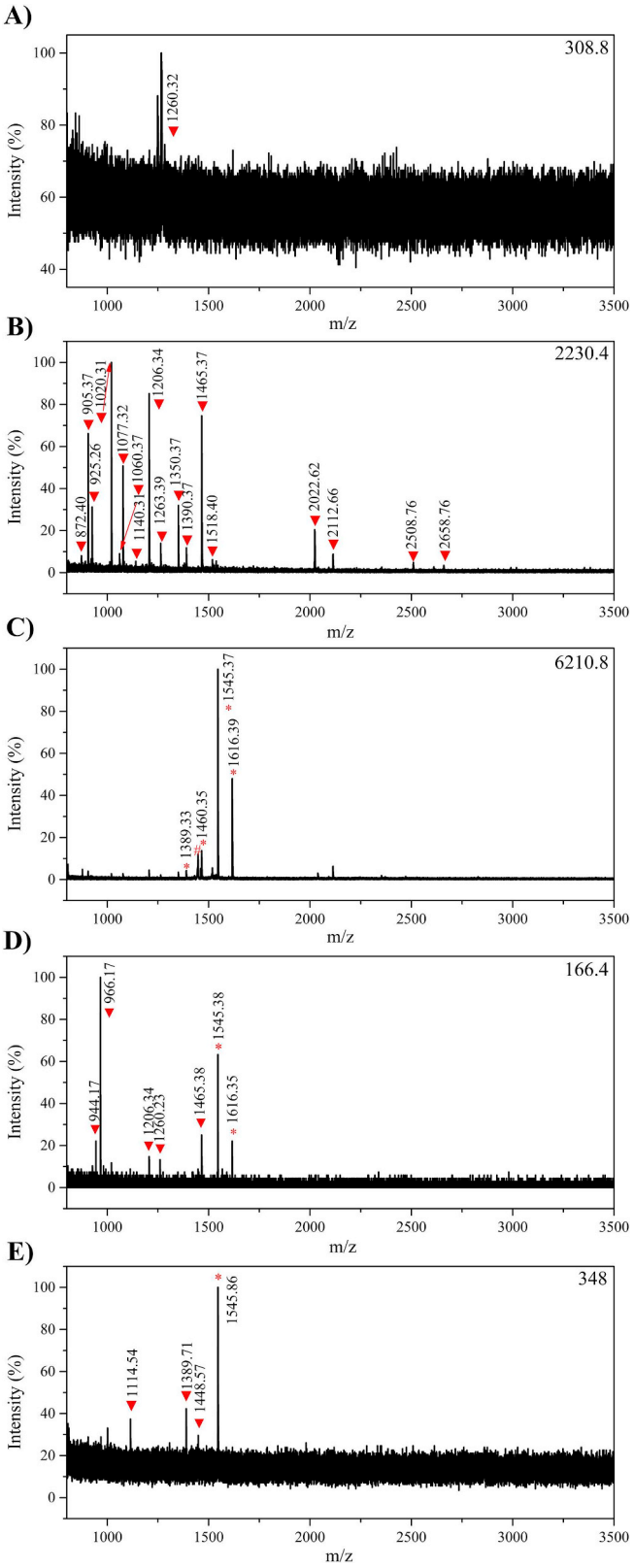

Fig. 4. Mass spectra of diluted human serum solution treated with different materials: A. Before enrichment; B. low-abundance peptides enriched in the first step; C. phosphopeptides captured in the second step; D. ZipTipC18; E. TiO_2. "▼" represents low-abundance peptides, "*" represents phosphopeptides; "#" represents dephosphorylate fragments of phosphopeptides. The number in the upper right corner represents the strongest peak intensity.

Table 2
Comparison of enrichment performance of the prepared Fe_3O_4/GO nanocomposites in this work with other bifunctional materials for low-abundance peptides and/or phosphopeptides.

Typical materials	Amount (μg)	Separation mode[a]	BSA digests	LODs (M)[b]	Selectivity (X: Y: Z)[c]	Application (Tryptic digests)	Ref.
r-GO-SnO_2	400	CS	36 peptides	4×10^{-10}	0 : 1: 25	BSA; β-Casein; Human serum	[37]
CeO_2/SiO_2–C_8 Janus fiber	400	CS	23 peptides	1×10^{-9}	0 : 1: 500	BSA; β-Casein; Human serum	[38]
Fe_3O_4/G/$LaPO_4$ (LaGM)	350	MS	16 peptides	1×10^{-9}	0 : 1: 50	BSA; β-Casein; Human urine; Human serum	[39]
Ti-MMSS	300	MS	13 peptides	NM	0 : 1: 100	BSA; α-Casein; Human serum;	[51]
$CuFeMnO_4$ NSAP	100	MS	17 peptides	2×10^{-10}	1 : 1: 100	BSA; α/β-Casein; Nonfat milk; Human saliva; Human serum; A549 cell lysate	[52]
Fe_3O_4/GO	100	MS	17 peptides	2.5×10^{-11}	1 : 1: 100	BSA; Angiotensin II, α/β-Casein; Human urine; Nonfat milk; Human serum	This work

[a] CS: Centrifugal separation; MS: Magnetic separation; NM: Not mentioned.
[b] LODs: Limits of detection for phosphopeptides.
[c] X: α-Casein; Y: β-Casein; Z: BSA.

amino group of 2-MIM is able to provide enough OH^- ions to induce the hydrolysis of Fe^{2+} forming $Fe(OH)_2$ precipitates. At the same time, O_2 in the air oxidizes the partial fresh $Fe(OH)_2$ to Fe_3O_4 nanocrystals. In addition, the amine with negative charge can combine Fe^{2+} ions by electrostatic interaction, and its negative charges make the as-prepared Fe_3O_4 nanoparticles more uniform via electrostatic repulsion. Then, Fe_3O_4/GO probe materials were prepared by simple ultrasonic assisted method for sequential enrichment of low-abundance peptides and phosphopeptides in real biological sample. Thanks to the allied merit of hydrophilicity of GO sheets and the strong affinity as well as superparamagnetism of Fe_3O_4 nanoparticles, the multifunctional Fe_3O_4/GO probe displayed rapidly, selectively and sensitively towards target peptide enrichment in human serum, which performed better than TiO_2 and ZipTipC18 pipette tips. This is a new analytical application of Fe_3O_4/GO nanocomposites to low-abundance peptides including phosphopeptides. The findings introduce a new thought of designing and building a binary probe for isolating various peptides from real complex biological samples.

Declaration of competing interest

The authors declare that they have no conflict of interest.

Acknowledgements

This work was supported by the National Natural Science Foundation of China (Nos. 21874065, 91643105, 21577057), and the Natural Science Foundation of Jiangsu Province (BK20171335).

Appendix A. Supplementary data

Supplementary data to this article can be found online at https://doi.org/10.1016/j.talanta.2019.120437.

References

[1] M. Swami, Proteomics: a discovery strategy for novel cancer biomarkers, Nat. Rev. Cancer 10 (2010) 597.
[2] S. Suwal, M.K.H. Pflum, Phosphorylation-dependent kinase–substrate cross-linking, Angew. Chem. Int. Ed. 49 (2010) 1627–1630.
[3] T. Pawson, J.D. Scott, Protein phosphorylation in signaling - 50 years and counting, Trends Biochem. Sci. 30 (2005) 286–290.
[4] J.R. Yates, S. Speicher, P.R. Griffin, T. Hunkapiller, Peptide mass maps: a highly informative approach to protein identification, Anal. Biochem. 214 (1993) 397–408.
[5] H.Q. Qin, P. Gao, F.J. Wang, L. Zhao, J. Zhu, A.Q. Wang, T. Zhang, R.A. Wu, H.F. Zou, Highly efficient extraction of serum peptides by ordered mesoporous carbon, Angew. Chem. Int. Ed. 50 (2011) 12218–12221.
[6] G.H. Han, M.L. Ye, H.F. Zou, Development of phosphopeptide enrichment techniques for phosphoproteome analysis, Analyst 133 (2008) 1128–1138.
[7] G.L. Corthals, V.C. Wasinger, D.F. Hochstrasser, J.C. Sanchez, The dynamic range of protein expression: a challenge for proteomic research, Electrophoresis 21 (2000) 1104–1115.
[8] Y. Oda, T. Nagasu, B.T. Chait, Enrichment analysis of phosphorylated proteins as a tool for probing the phosphoproteome, Nat. Biotechnol. 19 (2001) 379–382.
[9] L.H. Reddy, J.L. Arias, J. Nicolas, P. Couvreur, Magnetic nanoparticles: design and characterization, toxicity and biocompatibility, pharmaceutical and biomedical applications, Chem. Rev. 112 (2012) 5818–5878.
[10] M. Zhao, C.H. Deng, X.M. Zhang, P.Y. Yang, Facile synthesis of magnetic metal organic frameworks for the enrichment of low-abundance peptides for MALDI-TOF MS analysis, Proteomics 13 (2013) 3387–3392.
[11] Z.C. Xiong, Y.S. Ji, C.L. Fang, Q.Q. Zhang, L.Y. Zhang, M.L. Ye, W.B. Zhang, H.F. Zou, Facile preparation of core–shell magnetic metal–organic framework nanospheres for the selective enrichment of endogenous peptides, Chem. Eur J. 20 (2014) 7389–7395.
[12] H.M. Chen, S.S. Liu, H.L. Yang, Y. Mao, C.H. Deng, X.M. Zhang, P.Y. Yang, Selective separation and enrichment of peptides for ms analysis using the microspheres composed of Fe_3O_4@nSiO_2 core and perpendicularly aligned mesoporous SiO_2 shell, Proteomics 10 (2010) 930–939.
[13] G.T. Zhu, X.S. Li, Q. Gao, N.W. Zhao, B.F. Yuan, Y.Q. Feng, Pseudomorphic synthesis of monodisperse magnetic mesoporous silica microspheres for selective enrichment of endogenous peptides, J. Chromatogr. A 1224 (2012) 11–18.
[14] H.M. Chen, C.H. Deng, Y. Li, Y. Dai, P.Y. Yang, X.M. Zhang, A facile synthesis approach to C_8-functionalized magnetic carbonaceous polysaccharide microspheres for the highly efficient and rapid enrichment of peptides and direct MALDI-TOF-MS

Analysis, Adv. Mater. 21 (2009) 2200–2205.
[15] H.M. Chen, X.Q. Xu, N. Yao, C.H. Deng, P.F. Yang, X.M. Zhang, Facile synthesis of C_8-functionalized magnetic silica microspheres for enrichment of low-concentration peptides for direct MALDI-TOF MS analysis, Proteomics 8 (2008) 2778–2784.
[16] L.L. Sun, Q. Zhao, G.J. Zhu, Y. Zhou, T.T. Wang, Y.G. Shan, K.G. Yang, L. Zhen, L.H. Zhang, Y.K. Zhang, Octyl-functionalized hybrid magnetic mesoporous microspheres for enrichment of low-concentration peptides prior to direct analysis by matrix-assisted laser desorption/ionization time-of-flight mass spectrometry, Rapid Commun. Mass Spectrom. 25 (2011) 1257–1265.
[17] P. Yin, N.R. Sun, C.H. Deng, Y. Li, X.M. Zhang, P.Y. Yang, Facile preparation of magnetic graphene double-sided mesoporous composites for the selective enrichment and analysis of endogenous peptides, Proteomics 13 (2013) 2243–2250.
[18] Q. Liu, J.B. Shi, M.T. Cheng, G.L. Li, D. Cao, G.B. Jiang, Preparation of graphene-encapsulated magnetic microspheres for protein/peptide enrichment and MALDI-TOF MS analysis, Chem. Commun. 48 (2012) 1874–1876.
[19] H. Ünal, J.H. Niazi, Carbon nanotube decorated magnetic microspheres as an affinity matrix for biomolecules, J. Mater. Chem. B 1 (2013) 1894–1902.
[20] W.F. Ma, Y. Zhang, L.L. Li, L.J. You, P. Zhang, Y.T. Zhang, J.M. Li, M. Yu, J. Guo, H.J. Lu, C.C. Wang, Tailor-made magnetic Fe_3O_4@mTiO_2 microspheres with a tunable mesoporous anatase shell for highly selective and effective enrichment of phosphopeptides, ACS Nano 6 (2012) 3179–3188.
[21] W.F. Ma, C. Zhang, Y.T. Zhang, M. Yu, J. Guo, Y. Zhang, H.J. Lu, C.C. Wang, Magnetic MSP@ZrO_2 microspheres with yolk−shell structure: designed synthesis and application in highly selective enrichment of phosphopeptides, Langmuir 30 (2014) 6602–6611.
[22] G. Cheng, J.L. Zhang, Y.L. Liu, D.H. Sun, J.Z. Ni, Synthesis of novel Fe_3O_4@SiO_2@CeO_2 microspheres with mesoporous shell for phosphopeptide capturing and labeling, Chem. Commun. 47 (2011) 5732–5734.
[23] Y.Y. Hong, C.L. Pu, H.L. Zhao, Q.Y. Sheng, Q.L. Zhan, M.L. Lan, Yolk-shell magnetic mesoporous TiO_2 microspheres with flowerlike NiO nanosheets for highly selective enrichment of phosphopeptides, Nanoscale 9 (2017) 16764–16772.
[24] J. Lu, Y. Li, C.H. Deng, Facile synthesis of zirconium phosphonate-functionalized magnetic mesoporous silica microspheres designed for highly selective enrichment of phosphopeptides, Nanoscale 3 (2011) 1225–1233.
[25] X.Q. Xu, C.H. Deng, M.X. Gao, P.Y. Yang, X.M. Zhang, Synthesis of magnetic microspheres with immobilized metal ions for enrichment and direct determination of phosphopeptides by matrix-assisted laser desorption ionization mass spectrometry, Adv. Mater. 18 (2006) 3289–3293.
[26] N.R. Sun, C.H. Deng, Y. Li, X.M. Zhang, Size-exclusive magnetic graphene/mesoporous silica composites with titanium(IV)-immobilized pore walls for selective enrichment of endogenous phosphorylated peptides, ACS Appl. Mater. Interfaces 6 (2014) 11799–11804.
[27] Z.G. Wang, J.L. Zhang, D.H. Sun, J.Z. Ni, Novel Ti^{4+}-chelated magnetic nanostructured affinity microspheres containing n-methylene phosphonic chitosan for highly selective enrichment and rapid separation of phosphopeptides, J. Mater. Chem. B 2 (2014) 6886–6892.
[28] J. Su, X.W. He, L.X. Chen, Y.K. Zhang, Adenosine phosphate functionalized magnetic mesoporous graphene oxide nanocomposite for highly selective enrichment of phosphopeptides, ACS Sustain. Chem. Eng. 6 (2018) 2188–2196.
[29] X.Y. Long, Q. Song, H.Z. Lian, Development of magnetic $LuPO_4$ microspheres for highly selective enrichment and identification of phosphopeptides for MALDI-TOF MS analysis, J. Mater. Chem. B 3 (2015) 9330–9339.
[30] Q.H. Min, S.Y. Li, X.Q. Chen, E.S. Abdel-Halim, L.P. Jiang, J.J. Zhu, Magnetite/ceria-codecorated titanoniobate nanosheet: a 2D catalytic nanoprobe for efficient enrichment and programmed dephosphorylation of phosphopeptides, ACS Appl. Mater. Interfaces 7 (2015) 9563–9572.
[31] Y.J. Chen, Z.C. Xiong, L. Peng, Y.Y. Gan, Y.M. Zhao, J. Shen, J.H. Qian, L.Y. Zhang, W.B. Zhang, Facile Preparation of core-shell magnetic metal-organic framework nanoparticles for the selective capture of phosphopeptides, ACS Appl. Mater. Interfaces 7 (2015) 16338–16347.
[32] J.Q. Zhou, Y.L. Liang, X.W. He, L.X. Chen, Y.K. Zhang, Dual-functionalized magnetic metal-organic framework for highly specific enrichment of phosphopeptides, ACS Sustain. Chem. Eng. 5 (2017) 11413–11421.
[33] Y.T. Zhang, L.L. Li, W.F. Ma, Y. Zhang, M. Yu, J. Guo, H.J. Lu, C.C. Wang, Two-in-one strategy for effective enrichment of phosphopeptides using magnetic mesoporous γ-Fe_2O_3 nanocrystal clusters, ACS Appl. Mater. Interfaces 5 (2013) 614–621.
[34] H.Y. Zhong, X. Xiao, S. Zheng, W.Y. Zhang, M.G. Ding, H.Y. Jiang, L.L. Huang, J. Kang, Mass spectrometric analysis of mono- and multi-phosphopeptides by selective binding with $NiZnFe_2O_4$ magnetic nanoparticles, Nat. Commun. 4 (2013) 1656–1662.
[35] X.Y. Long, J.Y. Li, D. Sheng, H.Z. Lian, Spinel-type manganese ferrite ($MnFe_2O_4$) microspheres: a novel affinity probe for selective and fast enrichment of phosphopeptides, Talanta 166 (2017) 36–45.
[36] Y.G. Guo, J.S. Hu, L.J. Wan, Nanostructured materials for electrochemical energy conversion and storage devices, Adv. Mater. 20 (2008) 2878–2887.
[37] W. Ma, F. Zhang, L.P. Li, S. Chen, L.M. Qi, H.W. Liu, Y. Bai, Facile synthesis of mesocrystalline SnO_2 nanorods on reduced graphene oxide sheets: an appealing multifunctional affinity probe for sequential enrichment of endogenous peptides and phosphopeptides, ACS Appl. Mater. Interfaces 8 (2016) 35099–35105.
[38] N. Lv, Z.G. Wang, W.Z. Bi, G.M. Li, J.L. Zhang, J.Z. Ni, C_8-modified CeO_2//SiO_2 janus fibers for selective capture and individual MS detection of low-abundance peptides and phosphopeptides, J. Mater. Chem. B 4 (2016) 4402–4409.
[39] G. Cheng, Z.G. Wang, Y.L. Liu, J.L. Zhang, D.H. Sun, J.Z.A. Ni, Graphene-based multifunctional affinity probe for selective capture and sequential identification of different biomarkers from biosamples, Chem. Commun. 48 (2012) 10240–10242.
[40] N.A. Zubir, C. Yacou, J. Motuzas, X.W. Zhang, J.C.D. Costa, Structural and functional investigation of graphene oxide-Fe_3O_4 nanocomposites for the heterogeneous fenton-like reaction, Sci. Rep. 4 (2014) 4594–4602 D..
[41] D.L. Zhao, H.Y. Zhu, C.N. Wu, S.J. Feng, A. Alsaedi, T. Hayat, C.L. Chen, Facile synthesis of magnetic Fe_3O_4/graphene composites for enhanced U(VI) sorption, Appl. Surf. Sci. 444 (2018) 691–698.
[42] F. Vereda, J. De-Vicente, R. Hidalog-Alvarez, Oxidation of ferrous hydroxides with nitrate: a versatile method for the preparation of magnetic colloidal particles, J. Colloid Interface Sci. 392 (2013) 50–56.
[43] P. Tartaj, M.P. Morales, S. Veintemillas-Verdaguer, T. Gonzalez-Carreno, C.J. Serna, The preparation of magnetic nanoparticles for applications in biomedicine, J. Phys. D Appl. Phys. 36 (2003) 182–197.
[44] H. Deng, X.L. Li, Q. Peng, X. Wang, J.P. Chen, Y.D. Li, Monodisperse magnetic single-crystal ferrite microspheres, Angew. Chem. Int. Ed. 44 (2005) 2782–2785.
[45] Z.C. Xu, C.M. Shen, Y.L. Hou, H.J. Gao, S.H. Sun, Oleylamine as both reducing agent and stabilizer in a facile synthesis of magnetite nanoparticles, Chem. Mater. 21 (2009) 1778–1780.
[46] D. Amara, I. Felner, I. Nowik, S. Margel, Synthesis and characterization of Fe and Fe_3O_4 nanoparticles by thermal decomposition of triiron dodecacarbony, Colloids Surf., A 339 (2009) 106–110.
[47] N.J. Tang, W. Zhong, H.Y. Jiang, Nanostructured magnetite (Fe_3O_4) thin films prepared by sol-gel method, J. Magn. Magn. Mater. 282 (2004) 92–95.
[48] S. Laurent, D. Forge, M. Port, A. Roch, C. Robic, L. Vander Elst, R.N. Muller, Magnetic iron oxide nanoparticles: synthesis, stabilization, vectorization, physicochemical characterizations, and biological applications, Chem. Rev. 108 (2008) 2064-2011.
[49] E. Matijević, R.S. Sapieszko, J.B. Melville, Ferric hydrous oxide sols I. Monodispersed basic iron(III) sulfate particles, J. Colloid Interface Sci. 50 (1975) 567–581.
[50] D.L.A. de Faria, S. Venaüncio Silva, M.T. de Oliveira, Raman microspectroscopy of some iron oxides and oxyhydroxides, J. Raman Sepctrosc. 28 (1997) 873–878.
[51] X.S. Li, G.T. Zhu, Y. Zhao, B.F. Yuan, L. Guo, Y.Q. Feng, Titanium-containing magnetic mesoporous silica spheres: effective enrichment of peptides and simultaneous separation of nonphosphopeptides and phosphopeptides, J. Sep. Sci. 35 (2012) 1506–1513.
[52] X.Y. Long, Z.J. Zhang, J.Y. Li, D. Sheng, H.Z. Lian, Controllable preparation of $CuFeMnO_4$ nanospheres as a novel multifunctional affinity probe for efficient adsorption and selective enrichment of low-abundance peptides and phosphopeptides, Anal. Chem. 89 (2017) 10446–10453.